www.acsnano.org

# **Exploring Excited State Landscapes with Surface Enhanced Hyper-Raman Spectroscopy**

Aruna Chandran and Jon P. Camden\*



Downloaded via UNIV OF NOTRE DAME on May 13, 2025 at 14:09:07 (UTC). See https://pubs.acs.org/sharingguidelines for options on how to legitimately share published articles.

Cite This: ACS Nano 2024, 18, 20827-20834

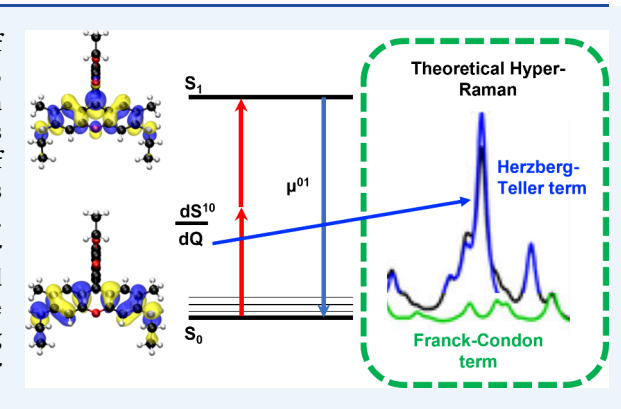


**ACCESS** I

Metrics & More

Article Recommendations

ABSTRACT: In this Perspective, we provide a historical overview of the surface-enhanced hyper-Raman scattering (SEHRS) effect, describe its essential components, highlight the close connection between theory and experiment in several vignettes, and discuss recent analytical applications. SEHRS, the two-photon analog of surface-enhanced Raman scattering (SERS), is a spontaneous nonlinear scattering exhibited by molecules in a plasmonic field. Hyper Raman provides distinctive information on the molecular vibrations and electronic excited states of analytes. A 40-year old mystery surrounding the SEHRS spectra of R6G is used to illustrate the power of SEHRS to explore excited electronic states, revealing how non-Condon effects can influence the two-photon molecular properties. The exceptionally large enhancement factors (>10<sup>13</sup>)



obtained from SEHRS enable the analysis of single molecules and molecules at very low concentrations. This high sensitivity is further augmented by an increased sensitivity to chemical effects, allowing SEHRS to probe changes in the local environment and the orientation of surface ligands. As most SEHRS experiments employ near-infrared (NIR) and short-wave infrared (SWIR) light, it also holds promise for bioimaging studies. Before concluding, we discuss future directions and challenges for the field as it moves forward.

**KEYWORDS:** surface-enhanced Raman scattering, surface-enhanced hyper Raman scattering, non-Condon effects, rhodamine 6G, hyper-Raman scattering

## **INTRODUCTION**

Half a century ago, McQuillen and Fleishmann observed an anomalously intense Raman spectrum from pyridine on a roughened silver electrode. They attributed this increased signal to the increased surface area upon roughening; however, after a careful investigation, Jeanmaire and Van Duyne<sup>2</sup> realized that a different mechanism was needed to explain these observations, as the surface area increase alone could not account for the observed enhancements. The responsible effect is what we now call "surface-enhanced Raman scattering" or "SERS". Shortly thereafter, Moskovits<sup>3</sup> realized that SERS was fundamentally a plasmonic phenomenon, invoking surface plasmons in the roughened metal to explain the SERS enhancements. With the benefit of hindsight, the discovery of the SERS effect was the catalyst that propelled plasmonics into the mainstream by captivating a multidisciplinary group of scientists who were interested in understanding this effect and harnessing it to create advanced devices.

Almost immediately after the discovery of SERS, it was realized that surface enhancement could also augment nonlinear processes such as surface-enhanced coherent

antistokes Raman scattering (SE-CARS)<sup>4</sup> in 1979, surface-enhanced second harmonic generation (SE-SHG)<sup>5</sup> in 1980, and surface-enhanced hyper-Raman scattering (SEHRS)<sup>6,7</sup> in 1982. More recently, surface-enhanced femtosecond stimulated Raman spectroscopy (SE-FSRS)<sup>8</sup> and surface-enhanced second-hyper-Raman scattering (SE2HRS)<sup>9</sup> were demonstrated in 2011 and 2015 respectively. While these nonlinear processes do not enjoy the same widespread application that SERS does today, they are windows into both the electromagnetic and chemical effects that drive the surface enhancement process and have practical applications in both sensing and imaging.<sup>10</sup> Furthermore, the advancement of both laser sources and detectors has primed nonlinear analogs of SERS for a renaissance. In this Perspective, we focus on the SEHRS

Received: May 15, 2024 Revised: July 18, 2024 Accepted: July 23, 2024 Published: August 1, 2024





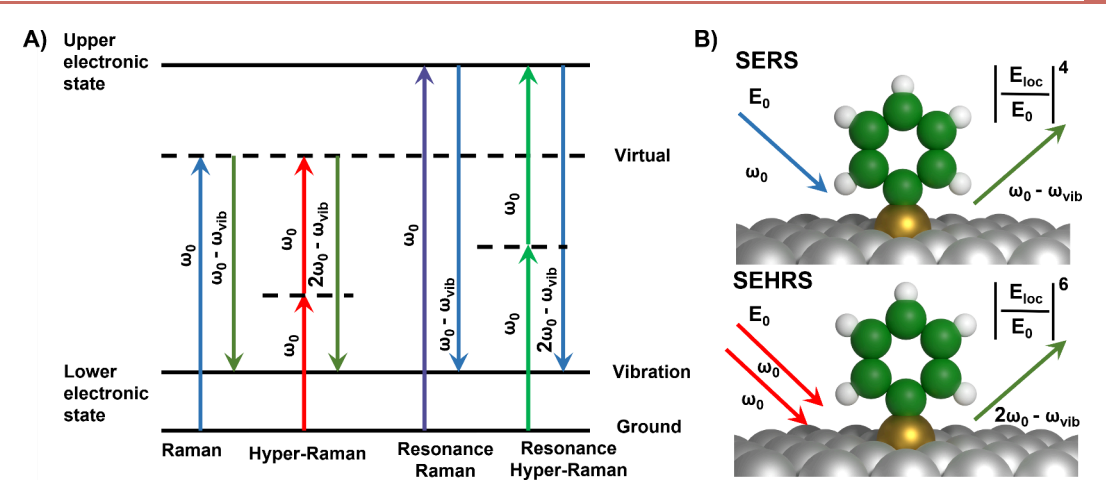


Figure 1. Overview of vibrational transitions, SERS, and SEHRS process. (A) Schematic representation of transitions associated with vibrational Raman, hyper-Raman, resonance Raman, and resonance hyper-Raman. (B) Schematic representation of surface-enhanced Raman (top) and surface-enhanced hyper-Raman (bottom) and the corresponding electromagnetic enhancement factors. Figure 1B created by S. Chowdhury and used with permission.

effect, beginning with a historical overview before summarizing state-of-the-art research in the field. Throughout the discussion, we provide several vignettes to illustrate the large and untapped potential of surface-enhanced nonlinear spectroscopies.

While the most consistent treatment of nonlinear processes proceeds from a quantum mechanical treatment of the susceptibility, 11 the spontaneous hyper-Raman effect is most easily approached using the dipole approximation. 12 Expanding the induced molecular dipole  $(\mu)$  in the applied field, we find that

$$\mu_{i} = 4\pi\epsilon_{0} \left( \alpha_{ij} E_{j} + \frac{1}{2} \beta_{ijk} E_{j} E_{k} + \frac{1}{6} \gamma_{ijkl} E_{j} E_{k} E_{l} \right)$$

$$\tag{1}$$

where  $\alpha$ ,  $\beta$ , and  $\gamma$  refer to the molecular polarizability, hyperpolarizability, and second hyperpolarizability respectively, and E is the applied electric field. If  $\alpha$  and  $\beta$  are further expanded in normal mode coordinates and a harmonic driving field is applied to eq 1, scattered frequencies appear at  $\omega_0$ ,  $\omega_0 \pm \omega_{\rm vib}$ ,  $2\omega_0$ ,  $2\omega_0 \pm \omega_{\rm vib}$ , where  $\omega_0$  is the laser frequency and  $\omega_{\rm vib}$  is the characteristic frequency of the material (Figure 1). This set of frequencies corresponds to Rayleigh, Raman, hyper-Rayleigh, and hyper-Raman scattering, all of which can be resonance enhanced when the laser frequency coincides with a molecular excited state.

Hyper-Raman scattering (HRS) was observed by Terhune, Maker, and Savage in 1965 by illuminating water and fused quartz with a high-power Ruby laser, 13 although the subsequent experimental progress was slow given the extreme weakness of the effect. Theoretical studies by Cyvin, Rauch, and Decius in the same year explored the symmetry properties, vibrational selection rules, and depolarization ratios for the hyper-Raman effect using the hyper-polarizability tensor. 14 These theoretical studies highlighted the complementary nature of hyper-Raman scattering by showing that silent vibrational modes, i.e. those that are both Raman and IR inactive, are hyper-Raman active. Early reviews of hyper-Raman were given by Ziegler<sup>15</sup> and Baranov and Bobovich, <sup>16</sup> both of which paid special attention to resonance effects, and a comprehensive review of the hyper-Raman effect was given by Kelley<sup>17</sup> in 2010. More recently, a review targeting SEHRS was given by Kneipp<sup>10</sup> in 2017.

Interestingly, SEHRS was reported very shortly after the discovery of SERS. In 1982 Chang, Dorain, and co-workers and Baranov and Bobovich<sup>7</sup> independently showed that hyper-Raman scattering was massively enhanced by combining analytes with silver colloids. Then in 1988 Van Duyne, Schatz, and co-workers<sup>18</sup> performed the most comprehensive early study of the SEHRS effect, combining both experiment and theory to study pyridine adsorbed onto Ag electrodes. Their work estimated the SEHRS enhancement factor ( $\sim 10^{13}$ ) and suggested that chemical enhancement effects are amplified when performing SEHRS, a feature that was later confirmed by theoretical work from Schatz and co-workers. 19 In 1999, shortly after the discovery of single-molecule SERS (SM-SERS), Kneipp and co-workers<sup>20</sup> reported that hyper-Raman enhancements could exceed 10<sup>20</sup> for resonant dye molecules such as crystal violet (CV), meaning that surface enhancement could overcome the inherent weakness of the HR process. Two additional milestones were achieved in 2006: Itoh and coworkers<sup>21</sup> showed that SEHRS is possible using a continuouswave near-infrared (CW-NIR) laser and Kelley and coworkers<sup>22</sup> demonstrated excellent SEHRS signals arising from a low-power laser source (<2 pJ per pulse, 82 MHz repetition rate, 1-2 ps pulse duration). Building on the early single molecule SERS work, Camden and co-workers<sup>23</sup> used the bianalyte isotopologue method to prove that SEHRS could be observed from single CV molecules in 2013.

**Applications of SEHRS.** Despite the proliferation of SERS applications through the years, SEHRS has mostly remained a laboratory curiosity. One particularly appealing aspect of nonlinear scattering is the potential to use near-infrared (NIR: 750-1000 nm) and short-wave infrared (SWIR: 1000-2000 nm) excitation. Multiphoton microscopy using NIR and SWIR mitigates the absorption losses, increases penetration through tissue, reduces scattering, and contributes to nondestructive high-resolution imaging.2 <sup>4</sup> The earliest imaging study using hyper-Raman measured the local pH in cells using NIR excitation (1064 nm), demonstrating the viability of biocompatible SEHRS-based nanosensors that were similar to well-established SERS-based methods.<sup>25</sup> The higher sensitivity of SEHRS toward surface charge and local environment enabled the measurement of pH over a wide range (pH = 2-12) using a single probe molecule, unlike

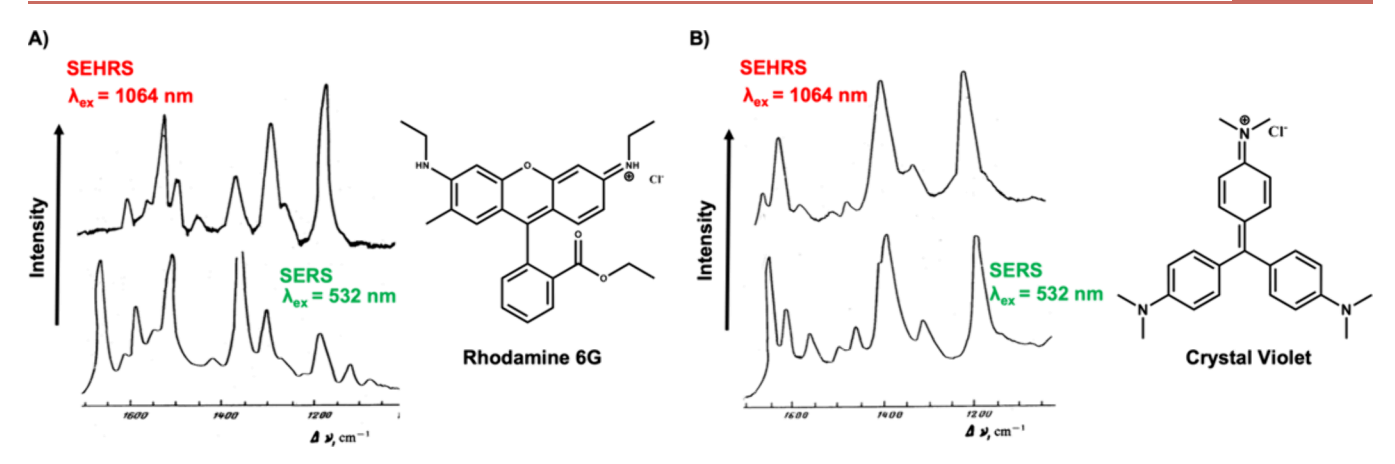


Figure 2. Comparing SEHRS and SERS of R6G and CV. SEHRS (1064 nm excitation) and SERS (532 nm excitation) spectra of rhodamine 6G (A) and crystal violet (B) adsorbed on silver hydrosol as reported in 1982. The SEHRS and SERS of R6G exhibit dramatic differences while the parallel comparison for CV shows the spectra are very similar. Figure adapted with permission from ref 7. Copyright 1982, Springer Nature.

previous two-photon fluorescence sensors which required multiple probes to cover a similar pH range.<sup>26</sup> In 2014 Turley and Camden extended SEHRS into the short-wave infrared (SWIR) to access the improved transparency and reduced scattering of the NIR-II (1000-1700 nm) window, showing that hyper-Raman scattering could be obtained using 1.5-1.8  $\mu$ m excitation.<sup>27</sup> This discovery was later employed to perform tissue imaging with SWIR SEHRS with high penetration depth and reduced scattering.<sup>28</sup> Kneipp and co-workers also employed 1550 nm excitation and SEHRS labels containing 2-naphthalenethiol to image the inside of macrophage cells, illustrating the bioanalytical potential of SEHRS.<sup>29</sup> More recently, the trace detection capabilities of SEHRS were explored by Trujillo et al., who used mercaptobenzoic acid functionalized nanoparticles to detect uranyl ion (UO<sub>2</sub><sup>2+</sup>) at 90 ppb (parts per billion), a detection limit that rivals similar SERS-based sensors.30

**Exploring a 40-Year-Old Mystery.** In 1982 Baranov and Bobovich encountered a curiosity when comparing the SEHRS  $(\lambda_{\rm ex}=1064~{\rm nm})$  and SERS  $(\lambda_{\rm ex}=532~{\rm nm})$  of rhodamine 6G (R6G) and crystal violet (CV) adsorbed on silver hydrosols: the SEHRS and SERS spectra of R6G are dramatically different while the SEHRS and SERS of CV are very similar (Figure 2). These experimental observations were the exact opposite of what they predicted using arguments based on the molecular symmetries!

In the vibronic theory of resonance hyper-Raman (RHR) scattering developed by Chung and Ziegler<sup>31</sup> the hyperpolarizability tensor can be divided into three terms: A, B, and C. The A-term, known as the Franck-Condon term, depends on the one- and two-photon transition moments evaluated at the equilibrium nuclear geometry. Strong A-term activity requires that both the one- and two-photon transitions be allowed, a condition that is always met in noncentrosymmetric molecules. Taken as a whole, rhodamine 6G has no symmetry and it is reasonable to expect its resonance Raman (RR) and RHR spectra are both dominated by A-term scattering, i.e., the RR and RHR are expected to be nearly identical. Contrary to this prediction, the experimentally measured SERS and SEHRS of R6G are significantly different (Figure 2A). On the other hand, crystal violet is centrosymmetric, meaning the excited electronic states have parity and the one- and two-photon transitions are mutually exclusive, i.e. if a transition is onephoton allowed it will not be two-photon allowed and vice versa. In this case, the RR spectrum will be dominated by Aterm activity, while the RHR will be B-term dominated, leading to dramatically different SERS and SEHRS spectra, which was not observed in experiment (Figure 2B). While this mystery has been resolved for R6G (vide infra) a complete explanation of the CV spectra is still lacking.

Beginning in 2010, Camden, Jensen and co-workers undertook a comprehensive wavelength-scanned study of the SEHRS spectra of R6G, comparing the experimental spectra to theoretical calculations including the contributions of non-Condon effects. 32 Figure 3 overviews the one- and two-photon absorption spectra of R6G in the region of the  $S_1 \leftarrow S_0$  and  $S_2$  $\leftarrow$  S<sub>0</sub> transitions and the molecular orbitals involved in these transitions. The  $S_1 \leftarrow S_0$  transition occurs from the antisymmetric HOMO to a symmetric LUMO; implying that the one-photon transition will be strongly allowed while the two-photon transition will be forbidden according to the parity selection rule. However, the presence of a weak feature in the experimental two-photon absorption spectrum (Figure 3A) for the  $S_1 \leftarrow S_0$  transition suggests a breakdown of the Condon approximation. This hypothesis is explored in Figure 3D, where the experimentally measured and theoretically simulated hyper-Raman spectrum on resonance with the  $S_1 \leftarrow S_0$  are compared. The contribution of the Franck-Condon (A) and Herzberg-Teller ( $B_1$  and  $B_2$ ) terms to the simulated spectra is given by the green, red, and blue traces, respectively. Upon excitation at 1030 nm, most of the spectral intensity arises from B2-term scattering, with only a minor contribution from A-term scattering. The smallness of the two-photon dipole transition moment (S10) means that vibrations which modify the transition moment (dS<sup>10</sup>/dQ, Q: nuclear coordinate) are featured prominently in the resonance hyper-Raman spectrum at this excitation energy as they are the modes that promote vibronic mixing.

Further insight into the origin of non-Condon effects and the selective enhancement of certain vibrational modes can be obtained by looking at the molecular orbitals. Figure 3C illustrates the changes in the orbitals induced by vibration along the 1535 cm<sup>-1</sup> coordinate, i.e. the vibronic mixing. This particular mode was selected as it is a very intense peak in the SEHRS when on resonance with  $S_1 \leftarrow S_0$ . The 1535 cm<sup>-1</sup> mode, being antisymmetric, can perturb the ground state

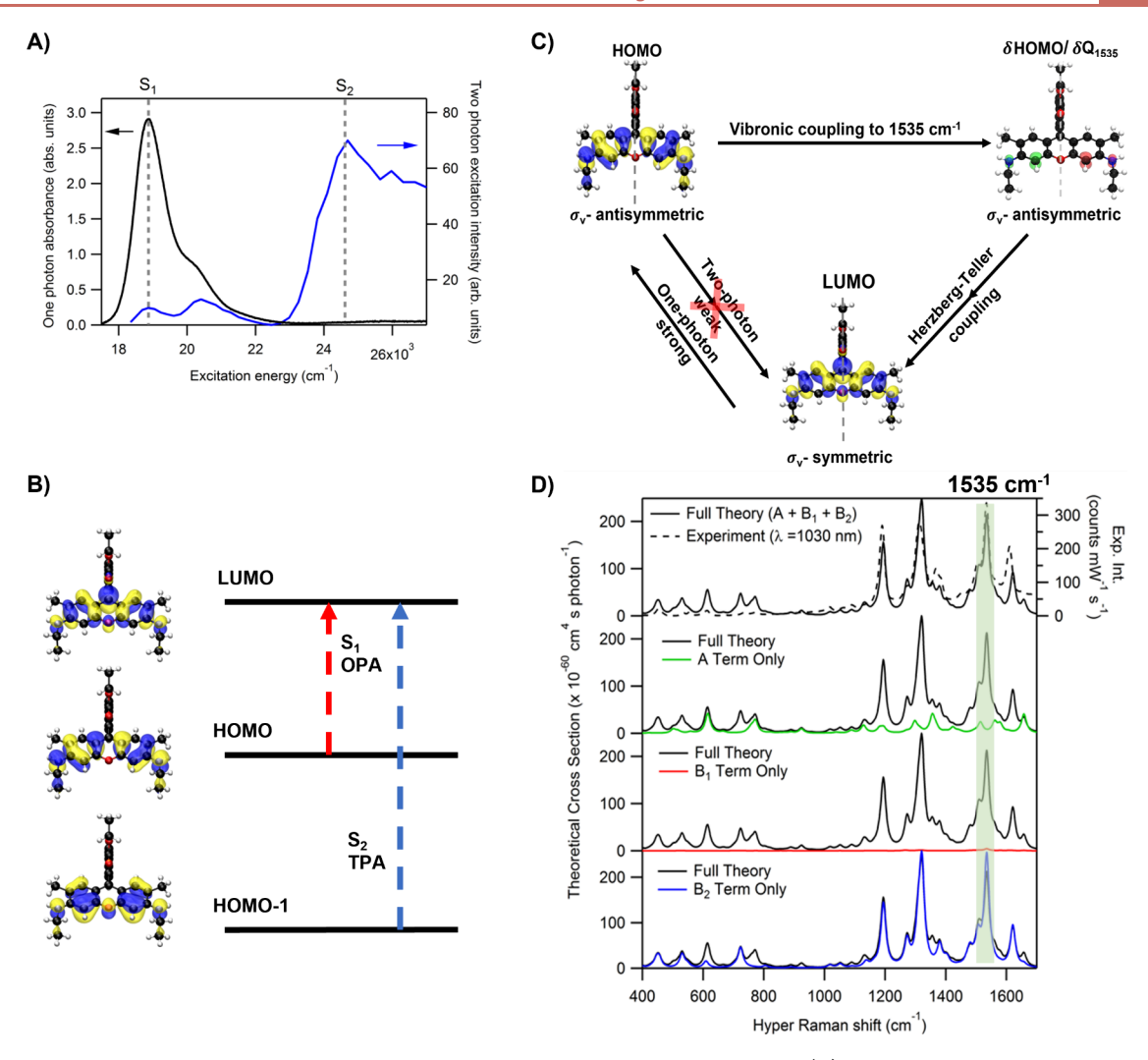


Figure 3. Overview of electronic transitions, hyper-Raman, and non-Condon effects in R6G. (A) One-photon absorbance and two-photon excitation spectra for R6G.  $S_1$  is strongly one-photon and weakly two-photon accessible while  $S_2$  is only two-photon accessible. (B) Molecular orbitals involved in the  $S_1 \leftarrow S_0$  (one photon allowed) and  $S_2 \leftarrow S_0$  (two photon allowed) electronic transitions in the R6G. (C) Detailed view of the vibronic (Herzberg–Teller) mixing induced by the 1535 cm<sup>-1</sup> vibrational mode in  $S_1 \leftarrow S_0$ . The two-photon transition from HOMO to LUMO is parity forbidden (asymmetric HOMO, symmetric LUMO) but vibronic coupling of 1535 cm<sup>-1</sup> introduces asymmetric changes to the HOMO, increasing the two-photon transition to the symmetric LUMO. (D) Comparison of experimental and calculated resonance hyper-Raman spectra excited at 1030 nm. The theoretical spectra are further decomposed into Franck—Condon (Aterm, green) and Herzberg—Teller ( $S_1$ - and  $S_2$ -terms, red and blue). In resonance with  $S_1$ , the hyper-Raman spectrum is dominated by the non-Condon scattering arising from the  $S_2$  term. Figure adapted with permission from ref 32. Copyright 2013, ACS Publications.

antisymmetrically, resulting in a more symmetric HOMO. This perturbed HOMO increases the strength of the two-photon transition to the LUMO. Once excited to the symmetric LUMO, a one-photon transition back to HOMO is allowed as per the parity selection rule. These theoretical investigations offer interesting physical insights into how specific vibrations can influence two-photon properties via Herzberg-Teller contributions. In this transition, one side of the xanthene utilizes the  $\pi$  backbone to act as an electron donating group (Figure 3C, right, red), transferring electron density to the other side of the xanthene ring, which serves as an electronaccepting group (Figure 3C, right, green). In this context, R6G is exhibiting the characteristics of a push-pull chromophore,<sup>33</sup> whereby the presence of both donating and accepting groups in the same molecule enhances the nonlinear optical properties. In conclusion, employing resonance hyper-Raman experiments and simulations, the longstanding R6G SEHRS mystery was resolved and, more importantly, this work

suggests that non-Condon effects can be used to rationally design chromophores with enhanced nonlinear molecular properties.

Unlike R6G, the SERS and SEHRS spectra of CV on resonance with its first electronic excited state are almost identical, indicating that CV's increased symmetry does not result in the expected difference in selection rules between RR and RHR. To understand the mechanism underpinning excited state contributions to the two-photon spectroscopy of CV, a combined experimental and theoretical study of the wavelength scanned SERS and SEHRS spectra in vicinity of  $S_1$  was performed.<sup>34</sup> The theoretical spectra neglected solvent and nanoparticle interactions, where CV adopts a near  $D_3$  symmetry. The similarity of RR and RHR in experiments and simulations suggests that spectra in the region of  $S_1$  is indeed dominated by A-term scattering from a single state, or a set of nearly degenerate states. However, a closer comparison shows there is a significant discrepancy for the vibrational

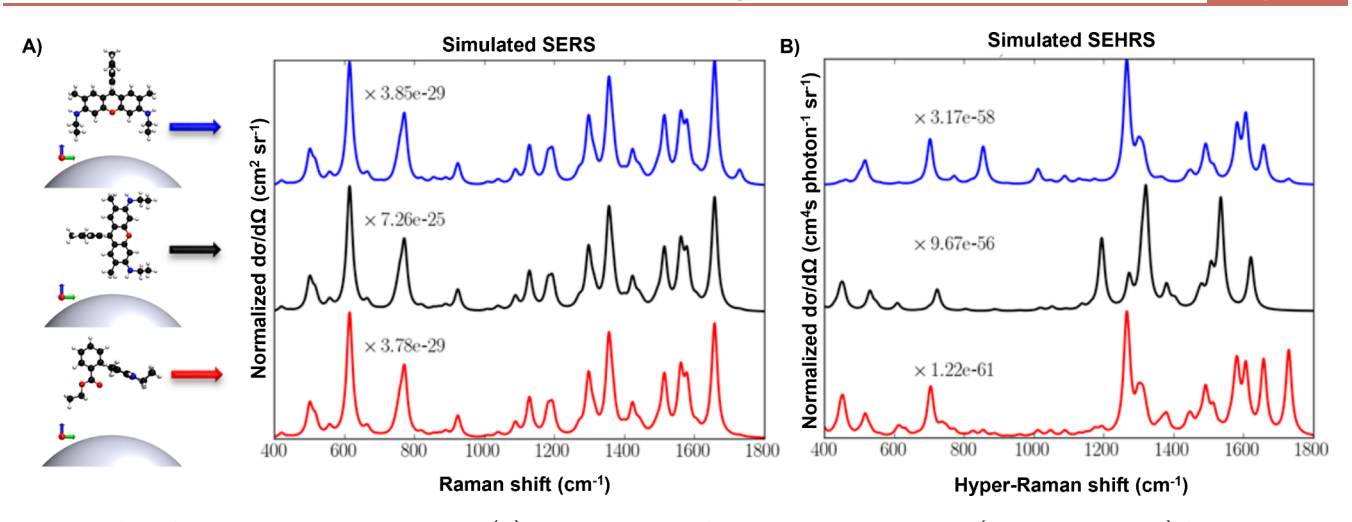


Figure 4. Effect of adsorbate geometry on SEHRS. (A) Simulated SERS of R6G on resonance with S1 (excitation: 532 nm) for three extreme molecular orientation with respect to nanoparticle surface. The relative mode intensities are not sensitive to orientation as the polarizability tensor directions are determined by the electronic state not the vibrational mode. (B) Due to the presence of non-Condon scattering, the SEHRS spectra of R6G on resonance with  $S_1$  (excitation: 1064 nm) displays a significant difference in relative mode intensities for the three limiting geometries, allowing for determination of the adsorbate geometry. Figure adapted with permission from ref 38. Copyright 2017, ACS Publications.

modes at 1536, 1585, and 1620 cm<sup>-1</sup>, corresponding to C–C stretching and C–H bending modes in the aromatic rings. This discrepancy could arise from the lowering of symmetry either due to interaction with the environment or the possible existence of multiple species with different symmetries.<sup>35</sup> To study the interactions with the environment, the SEHRS spectra from CV in different solvents were analyzed, but the resulting spectra are nearly identical indicating that solvent effects are minor. These discrepancies are also observed in the second-hyper Raman scattering (SE2HRS) of CV,<sup>9</sup> illustrating that the complex interplay of electronic transitions and vibrational modes in CV is still not understood and future studies are needed to fully explain the RHR spectra.

Using SEHRS to Understand Molecular Orientation. Under nonresonant conditions, surface selection rules dictate that the SERS intensity is preferentially enhanced for vibrational modes containing components of the bond polarizability tensor normal to the nanoparticle surfaces as they align with the local electric field. As the different vibrational modes possess polarizability tensors depending on their symmetries, adsorbate orientation can be extracted from the SERS spectra.<sup>37</sup> However, under resonance Raman conditions, the polarizability tensors take on the character of the electronic excited state, regardless of the vibrational mode, and information on the adsorbate geometry is lost. However, if a molecule displays large non-Condon scattering, this impasse can be broken as the directionality of the transition dipole derivatives again allow for the determination of adsorbate orientation. Camden, Jensen, and co-workers employed these non-Condon effects in the SEHRS of R6G to determine the local adsorbate geometry on silver colloids.<sup>38</sup> Figure 4 shows the simulated SERS and SEHRS of R6G in resonance with S1 at three extreme molecular orientations with respect to the nanoparticle surface. While the simulated SERS spectra (Figure 4A) show a difference in the overall intensity, the intensity ratios between modes are identical. Hence, the determination of the orientation of R6G by comparing this model with experimental SERS data is nearly impossible. However, the simulated SEHRS spectra (Figure 4B) show dramatic changes as a function of orientation.

This orientation-dependent behavior in the SEHRS of R6G can be attributed to the strong non-Condon effects (B<sub>2</sub>-term) that dominate the hyper-Raman scattering of R6G when on resonance with S<sub>1</sub>. As discussed in the previous section, the transition to S<sub>1</sub> is one photon allowed and weakly two-photon allowed. For S<sub>1</sub>, the one photon transition moment is dominated by contributions from a single state orientated along the xanthene ring for all vibrational modes. Conversely, for the two-photon transition, the resonance hyper-Raman scattering gains intensity through the vibrationally coupled two-photon transition moment (dS10/dQ, Q: nuclear coordinate). This contribution from the two-photon transition moment differs in direction depending on the symmetry of the vibrational mode. Therefore, the hyperpolarizability tensor points in different directions for vibrational modes of different symmetry leading to orientation-dependent SEHRS. A comparison between the experimental SEHRS and simulated SEHRS enabled extraction of the absolute adsorbate geometry. Given that the local adsorbate geometry strongly influences the strength and sensitivity of molecule-plasmon coupled response, SEHRS is expected to be a synergistic probe of the underlying molecule-nanoparticle structures.

## **FUTURE CHALLENGES**

Benchmarking with Theory and Experiments. From the narrative so far, it is evident that a close connection between theory and experiment is necessary to interpret the nuances of hyper-Raman spectra. Unfortunately, the experiment-theory comparison becomes increasingly more complex as the molecular size increases and, even in the case of small molecules, a satisfactory agreement between theory and experiment cannot always be achieved. For instance, a study exploring the nonlinear Raman scattering of tris(2,2'-bipyridine)ruthenium(II) (Ru(bpy)<sub>3</sub><sup>2+</sup>) simulated the resonance hyper-Raman spectra using two different functionals when resonant with the metal-to-ligand charge transfer (MLCT) band:<sup>39</sup> a hybrid B3LYP functional and a range-separated LC-PBE exchange-correlation functional. There are significant differences when comparing the simulated spectra

obtained from these two functionals (Figure 5). For example, the peak at  $\sim$ 673 cm<sup>-1</sup> is best described by LC-PBE indicating

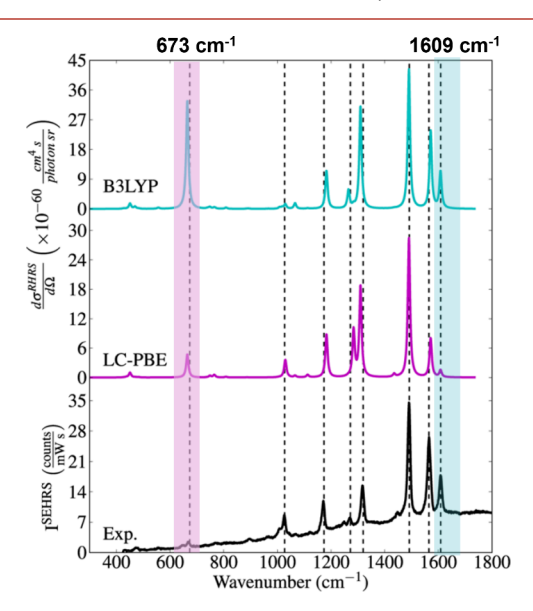


Figure 5. Comparing theoretical simulations of RHR to experiment. Simulated hyper-Raman spectra and experimental SEHRS spectra of Ru(bpy)<sub>3</sub><sup>2+</sup> excited at 940 nm on resonance with the metal-to-ligand charge transfer (MLCT) band. The peak at 673 cm<sup>-1</sup> (shaded pink) is best described by LCPBE and overestimated by B3LYP. In contrast, the peak at 1609 (shaded blue) is best described by B3LYP. Figure adapted with permission from ref 39. Copyright 2013, ACS Publications.

that the coupling of that mode, which involves significant stretching in the Ru–N bonds and ring breathing in the ligand is sensitive to the charge transfer character of the excited states involved whereas it was overestimated by B3LYP. Interestingly, the mode 1609 cm<sup>-1</sup> is best described by B3LYP which is characterized by ligand-centered C–C stretching and C–H wagging motion, and these modes may not be as sensitive to the MLCT characteristics. However, the limitations in the simulation approach, including the exchange-correlation functional and vibronic model used, demonstrate the difficulty of describing the changes in the intensity of modes observed in SEHRS spectra and highlight the need for improved computational methods and precisely controlled experimental systems.

Using SEHRS to Understand Chemical Enhancements. In SERS, the signal enhancement is attributed to two main mechanisms: the electromagnetic (EM) enhancement and chemical (CHEM) enhancement mechanisms. 40 While the EM mechanism arises from the increased electromagnetic field generated by excitation of the plasmon, the CHEM mechanism is postulated to arise from three different processes: enhancement due to ground-state chemical interactions, enhancements from molecular excitation resonances, and charge-transfer resonances. In practice, it is very difficult to disentangle the relative contributions of the CHEM or EM mechanism by experimental methods only. The EM enhancement in SEHRS, as discussed earlier (Figure 1B), is proportional to  $|E_{loc}|^6$ , but previous work suggests that the EM mechanism alone cannot account for the observed (1012 -10<sup>14</sup>) nonresonant SEHRS enhancement factors. <sup>19</sup> This suggests that the contribution from the chemical mechanism is higher and much more important in SEHRS when compared

to SERS, suggesting that hyper-Raman could be coupled with SERS to provide a comprehensive view of the CHEM enhancement factors in both spectroscopies.

## **CONCLUSIONS**

In this Perspective, we discuss the discovery of the SEHRS effect, a type of spontaneous nonlinear surface-enhanced spectroscopy, and its subsequent application to a variety of physical and analytical chemistry problems. As a multiphoton process, SEHRS provides information about the surface enhancement mechanisms and possesses selection rules that are complementary to SERS. Employing resonance effects, hyper-Raman spectroscopy additionally reports on multiple closely spaced electronic states and the two-photon properties of large and complex molecules. In other words, hyper-Raman provides another avenue for gaining insights into the molecular structure, electronic excited state landscapes, and vibrational modes of analytes and molecular probes. Its high sensitivity toward the molecular orientation and chemical environment helps capture small changes in the ligand surface structure that may be silent in linear spectroscopies such as SERS. Non-Condon effects can be studied experimentally and interpretation of the SEHRS data yields detailed information on how individual vibrational modes contribute to multiphoton properties such as two-photon absorption. The large SEHRS enhancement factors can yield high-quality spectra from very low concentration samples and even single molecules. As a two-photon process, the usage of low energy high penetrable wavelengths suggests it has promise in high-resolution bioimaging studies.

Looking forward, SEHRS is expected to provide detailed information on the chemical effects in surface-enhanced spectroscopies and benchmarks for emerging theoretical approaches to calculating nonlinear response properties. While it is unlikely that SEHRS will ever rival SERS for ease of use or widespread applicability, advancements in computational methods for electronic structure determination and lower-cost laser sources suggest that SEHRS is primed for a renaissance as it provides information that is either impossible or very difficult to obtain from other methods.

## **AUTHOR INFORMATION**

# **Corresponding Author**

Jon P. Camden – Department of Chemistry and Biochemistry, University of Notre Dame, Notre Dame, Indiana 46S56, United States; orcid.org/0000-0002-6179-2692; Email: jon.camden@nd.edu

#### Author

Aruna Chandran – Department of Chemistry and Biochemistry, University of Notre Dame, Notre Dame, Indiana 46556, United States

Complete contact information is available at: https://pubs.acs.org/10.1021/acsnano.4c06429

## **Author Contributions**

The manuscript was written through the contributions of all authors. All authors have approved the final version of the manuscript.

#### **Notes**

Any opinions, findings, and conclusions or recommendations expressed in this material are solely those of the authors and do not necessarily represent the views of the National Science Foundation.

The authors declare no competing financial interest.

#### **ACKNOWLEDGMENTS**

This work is supported by the National Science Foundation under grant number CHE-2404020.

## **ABBREVIATIONS**

R6G, rhodamine 6G; CV, crystal violet

#### **REFERENCES**

- (1) Fleischmann, M.; Hendra, P. J.; McQuillan, A. J. Raman spectra of pyridine adsorbed at a silver electrode. *Chemical physics letters* 1974, 26 (2), 163–166.
- (2) Jeanmaire, D. L.; Van Duyne, R. P. Surface Raman spectroelectrochemistry: Part I. Heterocyclic, aromatic, and aliphatic amines adsorbed on the anodized silver electrode. *Journal of electroanalytical chemistry and interfacial electrochemistry* **1977**, 84 (1), 1–20.
- (3) Moskovits, M. Surface roughness and the enhanced intensity of Raman scattering by molecules adsorbed on metals. *J. Chem. Phys.* **1978**, *69* (9), 4159–4161.
- (4) Chen, C.; De Castro, A.; Shen, Y.; DeMartini, F. Surface coherent anti-Stokes Raman spectroscopy. *Phys. Rev. Lett.* **1979**, 43 (13), 946.
- (5) Chen, C.; de Castro, A. R. B.; Shen, Y. Surface-enhanced second-harmonic generation. *Physical review letters* **1981**, *46* (2), 145.
- (6) Murphy, D.; Von Raben, K.; Chang, R.; Dorain, P. Surface-enhanced hyper-Raman scattering from SO32-adsorbed on Ag powder. *Chem. Phys. Lett.* **1982**, *85* (1), 43–47.
- (7) Baranov, A.; Bobovich, Y. S. Super-enhanced hyper-Raman scattering from dyes adsorbed on colloidal silver particles. *JETP Lett.* **1982**, *36* (8), 339–343.
- (8) Frontiera, R. R.; Henry, A.-I.; Gruenke, N. L.; Van Duyne, R. P. Surface-enhanced femtosecond stimulated Raman spectroscopy. *journal of physical chemistry letters* **2011**, 2 (10), 1199–1203.
- (9) Simmons, P. D., Jr; Turley, H. K.; Silverstein, D. W.; Jensen, L.; Camden, J. P. Surface-enhanced spectroscopy for higher-order light scattering: a combined experimental and theoretical study of second hyper-Raman scattering. *J. Phys. Chem. Lett.* **2015**, *6* (24), 5067–5071.
- (10) Madzharova, F.; Heiner, Z.; Kneipp, J. Surface enhanced hyper Raman scattering (SEHRS) and its applications. *Chem. Soc. Rev.* **2017**, 46 (13), 3980–3999.
- (11) Boyd, R. W. Nonlinear Optics; Academic Press: 2003.
- (12) Long, D. A. Non-Linear Raman Spectroscopy and Its Chemical Applications; Springer: Dordrecht, 1982.
- (13) Terhune, R.; Maker, P.; Savage, C. Measurements of nonlinear light scattering. *Phys. Rev. Lett.* **1965**, *14* (17), *6*81.
- (14) Cyvin, S.; Rauch, J.; Decius, J. Theory of hyper-Raman effects (nonlinear inelastic light scattering): Selection rules and depolarization ratios for the second-order polarizability. *J. Chem. Phys.* **1965**, 43 (11), 4083–4095.
- (15) Ziegler, L. Hyper-Raman spectroscopy. *Journal of Raman spectroscopy* **1990**, 21 (12), 769–779.
- (16) Baranov, A. V. e.; Bobovich, Y. S.; Petrov, V. I. Spectroscopy of resonance hyper-Raman scattering of light. *Soviet Physics Uspekhi* 1990, 33 (10), 812.
- (17) Kelley, A. M. Hyper-Raman scattering by molecular vibrations. *Annu. Rev. Phys. Chem.* **2010**, *61*, 41–61.
- (18) Golab, J.; Sprague, J.; Carron, K.; Schatz, G.; Van Duyne, R. A surface enhanced hyper-Raman scattering study of pyridine adsorbed onto silver: Experiment and theory. *J. Chem. Phys.* **1988**, 88 (12), 7942–7951.

- (19) Valley, N.; Jensen, L.; Autschbach, J.; Schatz, G. C. Theoretical studies of surface enhanced hyper-Raman spectroscopy: The chemical enhancement mechanism. *J. Chem. Phys.* **2010**, *133* (5), No. 054103.
- (20) Kneipp, K.; Kneipp, H.; Itzkan, I.; Dasari, R. R.; Feld, M. S. Surface-enhanced non-linear Raman scattering at the single-molecule level. *Chem. Phys.* **1999**, 247 (1), 155–162.
- (21) Itoh, T.; Ozaki, Y.; Yoshikawa, H.; Ihama, T.; Masuhara, H. Hyper-Rayleigh scattering and hyper-Raman scattering of dyeadsorbed silver nanoparticles induced by a focused continuous-wave near-infrared laser. *Applied Physics Letters* **2006**, *88* (8), No. 084102.
- (22) Leng, W.; Kelley, A. M. Surface-enhanced hyper-Raman spectra and enhancement factors for three SERS chromophores. SEHRS spectra on Ag films at pulse energies below 2 pJ. J. Am. Chem. Soc. 2006, 128 (11), 3492–3493.
- (23) Milojevich, C. B.; Mandrell, B. K.; Turley, H. K.; Iberi, V.; Best, M. D.; Camden, J. P. Surface-enhanced hyper-Raman scattering from single molecules. *J. Phys. Chem. Lett.* **2013**, *4* (20), 3420–3423.
- (24) Thimsen, E.; Sadtler, B.; Berezin, M. Y. Shortwave-infrared (SWIR) emitters for biological imaging: a review of challenges and opportunities. *Nanophotonics* **2017**, *6* (5), 1043–1054.
- (25) Kneipp, J.; Kneipp, H.; Wittig, B.; Kneipp, K. One-and two-photon excited optical pH probing for cells using surface-enhanced Raman and hyper-Raman nanosensors. *Nano Lett.* **2007**, *7* (9), 2819–2823
- (26) Gühlke, M.; Heiner, Z.; Kneipp, J. Combined near-infrared excited SEHRS and SERS spectra of pH sensors using silver nanostructures. *Phys. Chem. Chem. Phys.* **2015**, *17* (39), 26093–26100.
- (27) Turley, H.; Camden, J. A nonlinear approach to surface-enhanced sensing in the short-wave infrared. *Chem. Commun.* **2014**, 50 (12), 1472–1474.
- (28) Olson, J. E.; Yu, J. H.; Thimes, R. L.; Camden, J. P. Vibrational two-photon microscopy for tissue imaging: Short-wave infrared surface-enhanced resonance hyper-Raman scattering. *Journal of Biophotonics* **2022**, *15* (1), No. e202100158.
- (29) Heiner, Z.; Madzharova, F.; Živanović, V.; Kneipp, J. Bioprobing with nonresonant surface-enhanced hyper-Raman scattering excited at 1,550 nm. *J. Raman Spectrosc.* **2021**, 52 (2), 394–403.
- (30) Trujillo, M. J.; Camden, J. P. Utilizing Molecular Hyper-polarizability for Trace Analysis: A Surface-Enhanced Hyper-Raman Scattering Study of Uranyl Ion. ACS omega 2018, 3 (6), 6660–6664.
- (31) Chung, Y.; Ziegler, L. The vibronic theory of resonance hyper-Raman scattering. *J. Chem. Phys.* **1988**, 88 (12), 7287–7294.
- (32) Milojevich, C. B.; Silverstein, D. W.; Jensen, L.; Camden, J. P. Surface-enhanced hyper-Raman scattering elucidates the two-photon absorption spectrum of rhodamine 6G. *J. Phys. Chem. C* **2013**, *117* (6), 3046–3054.
- (33) Kelley, A. M.; Leng, W.; Blanchard-Desce, M. Resonance Hyper-Raman Scattering from Conjugated Organic Donor—Acceptor "Push—Pull" Chromophores with Large First Hyperpolarizabilities. *J. Am. Chem. Soc.* **2003**, *125* (35), 10520–10521.
- (34) Turley, H. K.; Hu, Z.; Silverstein, D. W.; Cooper, D. A.; Jensen, L.; Camden, J. P. Probing two-photon molecular properties with surface-enhanced hyper-Raman scattering: a combined experimental and theoretical study of crystal violet. *J. Phys. Chem. C* **2016**, *120* (37), 20936–20942.
- (35) Myers Kelley, A.; Shoute, L. C.; Blanchard-Desce, M.; Bartholomew, G. P.; Bazan, G. C. Resonance Raman, hyper-Raman, and hyper-Rayleigh depolarization ratios and symmetry breaking in solution. *Mol. Phys.* **2006**, *104* (8), 1239–1247.
- (36) Moskovits, M.; Suh, J. Surface selection rules for surface-enhanced Raman spectroscopy: calculations and application to the surface-enhanced Raman spectrum of phthalazine on silver. *J. Phys. Chem.* **1984**, *88* (23), 5526–5530.
- (37) Le Ru, E.; Meyer, S.; Artur, C.; Etchegoin, P.; Grand, J.; Lang, P.; Maurel, F. Experimental demonstration of surface selection rules for SERS on flat metallic surfaces. *Chem. Commun.* **2011**, *47* (13), 3903–3905.

- (38) Turley, H. K.; Hu, Z.; Jensen, L.; Camden, J. P. Surface-enhanced resonance hyper-Raman scattering elucidates the molecular orientation of rhodamine 6G on silver colloids. *J. Phys. Chem. Lett.* **2017**, *8* (8), 1819–1823.
- (39) Silverstein, D. W.; Milojevich, C. B.; Camden, J. P.; Jensen, L. Investigation of linear and nonlinear raman scattering for isotopologues of Ru (Bpy) 32+. *J. Phys. Chem. C* **2013**, *117* (40), 20855–20866.
- (40) Valley, N.; Greeneltch, N.; Van Duyne, R. P.; Schatz, G. C. A look at the origin and magnitude of the chemical contribution to the enhancement mechanism of surface-enhanced Raman spectroscopy (SERS): Theory and experiment. *J. Phys. Chem. Lett.* **2013**, *4* (16), 2599–2604.